Dynamic Proton Polarization in AlK Alum and $AlNH_4$ Alum*

PHILIP J. BENDT
Los Alamos Scientific Laboratory, University of California, Los Alamos, New Mexico 87544

(Received 13 July 1970)

Over 50% proton polarization has been attained in three sulfate alum crystals containing dilute Cr^{3+} ions, at 1 K and ~19.5 kG, with ~$\frac{1}{4}$-W microwave power. We measured polarization growth-rate curves, polarization as a function of magnetic field, proton line shapes and widths, and proton spin-lattice relaxation times. The theory of dynamic polarization for well-separated allowed and forbidden transitions applies to the alums. To obtain high proton polarization, the alums require about three times as much microwave power as lanthanum magnesium nitrate (LMN). A pure AlK alum had a very long proton relaxation time (1.3×10^4 sec at 0.96 K), making it a promising crystal for "storing" polarization. $AlNH_4$ alum should make useful polarized targets for low-energy scattering experiments, because it contains 1.97 times as much hydrogen by weight as LMN.

I. INTRODUCTION

In $AlK(SO_4)_2\cdot12H_2O$ and $AlNH_4(SO_4)_2\cdot12H_2O$, each Al ion is surrounded by six water molecules forming a regular octahedron, with an Al–H_2O separation of about 2 Å.[1] If a small fraction (<0.5%) of the diamagnetic Al is replaced with paramagnetic Cr^{3+} ions, the paramagnetic ions are dipolar coupled with the protons, forming a system suitable for dynamic proton polarization by the "solid effect."[2] Though Cr^{3+} has a spin $S=\frac{3}{2}$, the electron-paramagnetic-resonance (EPR) spectra are dominated by the $(-\frac{1}{2},\frac{1}{2})$ transition, especially when the (111) crystal planes are oriented perpendicular to the magnetic field.[3] An explanation of this was given by Bleaney,[4] who suggested that the zero-field Stark splitting is not quite constant throughout the mixed crystal; this smears out the EPR lines, except for the $(-\frac{1}{2},\frac{1}{2})$ transition.

We have studied dynamic proton polarization, and proton spin-lattice relaxation times, in four alum crystals, along with a lanthanum-magnesium-nitrate (LMN) crystal for comparison.[5] It is significant for target applications that the AlK and $AlNH_4$ alums contain more hydrogen by weight, 61 and 97%, respectively, than the commonly used LMN.

The full width at half-power of the EPR lines used for pumping dynamic polarization varied from 10 to 22 G, and the widths of the proton nuclear-magnetic-resonance (NMR) lines varied from 7 to 15 G. Since the allowed and "forbidden" EPR transitions are sufficiently well separated (~29 G) that only the tails of the EPR lines overlap, the theory of dynamic polarization in dipolar crystals by Jeffries[6] and Borghini[7] applies to the alums. Dynamic proton polarization in butanol and glycol[8] is explained with other models,[9] because of the broad EPR lines and short proton relaxation times encountered.

II. THEORY OF DYNAMIC PROTON POLARIZATION

We will outline the theory in the notation of Jeffries,[6] who devised a "shell-of-influence" model for the protons surrounding each paramagnetic ion. Moving outward from the ion, four radii are defined: r_1 is the closest ion-proton spacing determined by crystal structure (~2 Å in alums). The protons between r_1 and r_1' (~7 Å) are so close to the ion that the local magnetic field shifts the NMR frequency by more than a linewidth, and therefore their polarization is not measured. Next comes the radius r_2' (~10 Å) of the "diffusion barrier," inside of which protons do not come into equilibrium by rapid mutual spin flips, due to variation in the local field at different radii. Finally, the majority of protons (>95%) are located between r_2' and r_2, where $r_2=(\frac{4}{3}\pi N)^{-1/3}$ (N is the density of ions per cm^3). In our alum crystals, r_2 varied from 28 to 40 Å.

The n protons between r_1 and r_2' are relaxed directly by the ion at the center of the shell, with a relaxation time T_{1n}. The n' protons ($n'\gg n$) between r_2' and r_2 remain in internal equilibrium through rapid mutual spin flips. The n' protons have two relaxation mechanisms: coupling to the n protons across the diffusion barrier with a cross-relaxation time T_{12}, and "leakage" relaxation through paramagnetic impurities with a relaxation time T_{1nl}. Since the n' protons dominate the NMR spectrum, we identify the experimental proton relaxation time T_{1p} with the n' protons. We simplify Jeffries's equations, without introducing appreciable error, by letting T_{12} go to zero; the experimental relaxation time is then given by

$$T_{1p}^{-1}=(n/n')\,T_{1n}^{-1}+T_{1nl}^{-1}. \tag{1}$$

Protons are dynamically polarized by pumping "forbidden" transitions at the EPR frequencies $(\gamma_e\pm\gamma_p)H/2\pi$, where γ_e and γ_p are the ion and proton gyromagnetic ratios, and H is the magnetic field strength. Pumping the lower frequency polarizes protons parallel to the magnetic field, producing positive polarization, and pumping the higher frequency produces negative polarization. Allowed transitions at $\gamma_eH/2\pi$ are induced by a microwave field H_{1e} at the rate

$$W_1=(T_{2e}/2)\,(\gamma_eH_{1e})^2=S/2T_{1e}, \tag{2}$$

where T_{1e} and T_{2e} are the ion spin-lattice and transverse relaxation times. Measurements of T_{1e} are reported in PB. For T_{2e}, we use the expression $T_{2e}=(\gamma_e\delta H)^{-1}$, where δH is the half-width at half-power of the EPR

TABLE I. Properties of the crystals.

Crystal No.	1	2	3	4	LMN
Composition	AlK alum	AlK alum	$AlNH_4$ alum	$AlNH_4$ alum	LMN
Weight (mg)	460	501	330	290	357
Density (g/cm^3)[a]	1.757	1.757	1.64	1.64	2.00
Hydrogen density (% by weight)	5.10	5.10	6.23	6.23	3.17
Al:Cr ratio	435	215	380	590	100[b]
H:Cr ratio	10 440	5160	9120	14 160	2400[b]
Concentration	5.14[c]	10.39[c]	5.73[c]	3.69[c]	15.8[d]
Derivative peak-to-peak proton linewidth (G)	12	7	12	15	8
T_{1p} at 0.93 K (sec)	13 000	3950	3350	1350	1320
EPR linewidth (G)	20	15	22	10	6
T_{1e} at 0.96 K (msec)	2.5	2.0	3.0	2.8	11.5

[a] *Handbook of Chemistry and Physics*, 50th ed., edited by R. C. Weast (Chemical Rubber Publishing Co., Cleveland, Ohio, 1969).
[b] Nominal La:Nd and H:Nd ratios.
[c] Units of 10^{18} (Cr ions)/cm^3.
[d] Units of 10^{18} (Nd ions)/cm^3.

line. S is the EPR saturation factor

$$S=T_{1e}T_{2e}(\gamma_e H_{1e})^2. \tag{3}$$

We calculate H_{1e}^2 from an equation for a resonant cavity,

$$\overline{H_{1e}^2}=2UQ/3V\nu_e, \tag{4}$$

where U is the microwave power dissipated in the cavity in erg/sec, Q is the cavity figure of merit ($\sim$2000), V is the cavity volume (6.78 cm^3), and ν_e is the microwave frequency.

Forbidden transitions are induced at the rate $W_2=\sigma W_1$, where σ is a coupling parameter. Schmugge and Jeffries derive the following expression for σ:

$$\sigma=\tfrac{3}{10}(g\beta/H)^2(1/\langle r^6\rangle)$$
$$=\tfrac{3}{10}(g\beta/H)^2(1/r_1^3r_2^3), \tag{5}$$

where g is the ion g value for the particular crystal orientation, β is a Bohr magnetion, and $\langle r^6\rangle$ is the average of the sixth power of the variable radius in the shell-of-influence model. By integrating between r_1 and r_2, it can be shown that $\langle r^6\rangle^{-1}$ equals $(r_1r_2)^{-3}$. The value $(\frac{4}{3}\pi N)^{-1/3}$ seems reasonable for r_2. Agreement with the theory is not obtained if r_1 is taken to be the crystallographic distance. We suggest that this may be due to the large local dipole field of the ions at the nearest protons. We will use r_1 evaluated by Eq. (5) as a parameter determined by experiment. It is to be understood that, in our interpretation, r_1 does not stand for any defined crystallographic spacing between ions and protons.

The steady-state proton polarization p_s is given by

$$p_s\approx[P_0/(1+f)][S/(S+S_{1/2})], \tag{6}$$

where P_0 is the ion thermal-equilibrium polarization, f is the leakage factor, and $S_{1/2}$ is a constant which depends on the crystal properties and the magnetic field. The factor $S/(S+S_{1/2})$ is zero when the microwave power is zero, and 1 when the microwave power is infinite. We refer to $S/(S+S_{1/2})$ as the "microwave factor" for dynamic polarization.

Since the $(-\frac{1}{2},\frac{1}{2})$ transition dominates the Cr^{3+}-ion EPR spectra, and is the transition used to pump dynamic proton polarization, we assign the ion an effective spin $S'=\frac{1}{2}$, and write

$$P_0=\tanh(h\nu_e/2kT). \tag{7}$$

The leakage factor f is given by

$$f=(n'/N)(T_{1e}/T_{1p}), \tag{8}$$

where T_{1e} and T_{1p} are measured values. The proton density n' approximately equals the total proton density, and the latter was used to calculate f. The factor $S_{1/2}$ is given by

$$S_{1/2}=(2/\sigma)[T_{1e}/T_{1p}(1+f)]. \tag{9}$$

The proton polarization grows in with a single time constant τ,

$$p(t)=p_s[1-\exp(-t/\tau)]. \tag{10}$$

The value of τ is given by

$$\tau=T_{1p}[1+S/S_{1/2}(1+f)]^{-1}. \tag{11}$$

Dropping the factors $1+f$, which equal $\sim$1, Eqs. (6) and (11) can be combined to obtain an equation first published by Borghini[10]:

$$\tau/T_{1p}+p_s/p_0=B', \tag{12}$$

where the theoretical value $B'=1$ apparently assumes that the magnetic resonance is perfectly tuned. Putting experimental values into Eq. (12), we have always found $B'>1$.

We outline briefly how the theory of dynamic proton polarization was used to interpret our experimental results.

(a) The liquid-helium boil-off rate was used to determine the microwave power U, and the measured Q of the cavity and U were used in Eq. (4) to determine H_{1e}^2.

(b) The measured EPR linewidth δH and the measured T_{1e} were used in Eq. (3) to determine S.

(c) Equation (8) was used to calculate f, from measured values of T_{1e} and T_{1p}.

(d) We fitted polarization growth-rate curves to Eq. (10), thereby determining p_s and τ. B' was then calculated using Eq. (12).

(e) "Experimental values" of f, S, and p_s were put into Eq. (6), which was solved for $S_{1/2}$.

(f) Using $S_{1/2}$, Eq. (9) was solved for σ.

(g) Using the value of σ thus obtained and the value of r_2^{-3}, Eq. (5) was solved for r_1.

The accuracy of the measurements, and the ability of the theory to give consistent results with different crystal parameters, is indicated by the variation in the values of B' and r_1. The equations in this section may not apply to the LMN crystal, in which the ion relaxation is strongly phonon bottlenecked.

III. CRYSTALS AND MICROWAVE CAVITY

The crystal habit is to grow in the form of a regular octahedron, the large plane surfaces of which are equilateral triangles. The unit cell is cubic, and the triangular surfaces are {111} planes. Important properties of the crystals are listed in Table I. The Al:Cr ratio was determined by chemical analysis.[11] The crystals are described in more detail in PB.

From the crystals, irregular cylinders were cut, which contained two adjacent {111} plane surfaces as part of the "cylindrical" surface. The cylinders were ~1 cm long and ~0.6 cm in diameter. They were placed with the edge between {111} planes vertical, in a Kel-F holder in the center of a cylindrical microwave cavity, as shown in Fig. 1. The Kel-F holder served as a coil form for a four-turn vertical NMR coil.

The cylindrical microwave cavity was machined from OFHC copper. The 0.25-in.-diameter iris shown in Fig. 1 was chosen to provide moderately high Q and good coupling to the waveguide. The mechanical tuning rod was used in connection with an oscilloscope display of cavity modes, and could be used to spoil an unwanted overlapping mode, and occasionally to sharpen a wanted mode.

The cavity diameter was 2.045 cm, the length was 2.065 cm, and the volume was 6.78 cm^3. Since the wavelength of the microwaves was ~0.56 cm, each linear dimension was about four wavelengths, and cavity modes were high-order modes. Since the crystal dimensions were one to two wavelengths, the crystal was uniformly irradiated with microwave power, except for nodes in the standing-wave pattern. The average width of a strong cavity resonance was ~26 MHz at a frequency of 52 GHz, indicating the cavity Q equaled ~2000.

The microwave cavity and crystal could be rotated about a vertical axis from outside the cryostat. For dynamic proton polarization, the alum crystals were oriented with the (111) planes perpendicular to the external magnetic field **H**, as shown in Fig. 1. We also

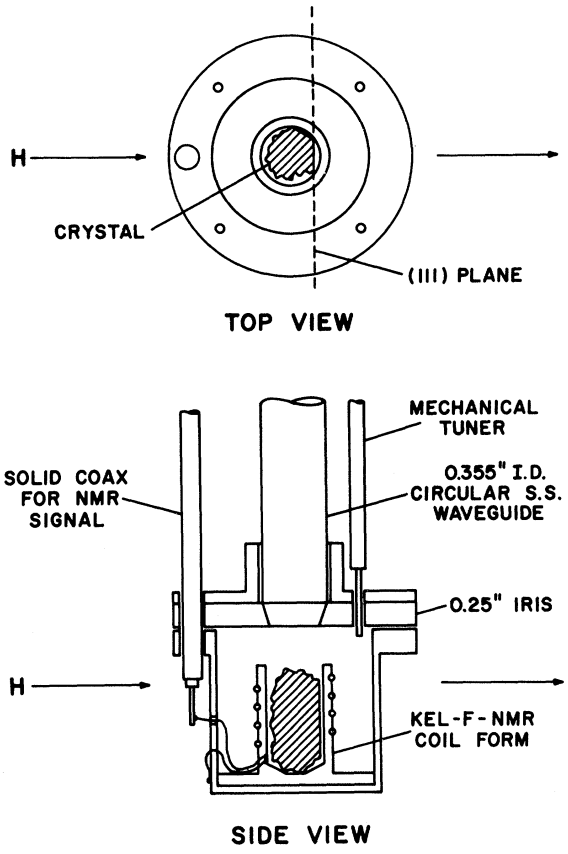

FIG. 1. Microwave cavity and Kel-F crystal holder used for dynamic-proton-polarization measurements.

polarized one alum crystal (No. 4) oriented with the (110) planes perpendicular to **H**. The LMN crystal was mounted with its c axis perpendicular to the magnetic field, which is the orientation in which the Nd^{3+}-ion g value is a maximum ($g=2.70$).

IV. APPARATUS

The crystal and microwave cavity were immersed in liquid helium, in a conventional batch-type ^4He cryostat, which was connected through a 6-in.-diameter pumping line to a 750-liter/sec mechanical pump. The microwave power dissipated in the liquid-helium bath was measured by a gas-flow meter on the pump exhaust. With 200 mW of microwave power, the helium-bath temperature was 1.00 K. The microwave cavity was centered in the 2.1-in. gap between pole tips of a 15-in.-pole-diameter electromagnet. The apparatus is the same as described in PB.

The forbidden EPR transitions were pumped with a 350-mW klystron, between 190 and 290 mW were delivered to the microwave cavity. A klystron stabilizer was used to lock the klystron frequency to a cavity mode. For the purpose of tuning the klystron and the magnetic field, reflected microwave power was detected with a crystal diode and displayed on an oscilloscope,

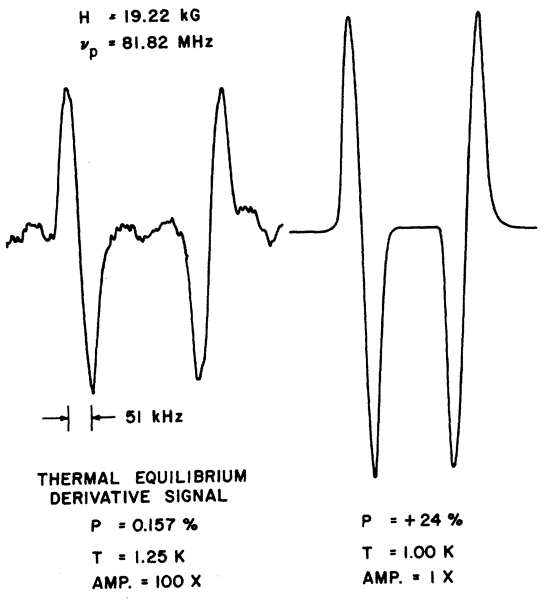

FIG. 2. Derivative of the proton resonance for AlK alum No. 1, at thermal equilibrium, and at 24% polarization. Each trace consists of an increasing frequency sweep on the left, followed by a decreasing frequency sweep.

by sweeping the klystron reflector voltage. We used the oscilloscope display to set the magnetic field so the frequency of an allowed EPR transition coincided with a cavity resonance. We shifted to a forbidden transition (not observable on the oscilloscope) by changing the magnetic field ~29 G.

A standard Q-meter circuit,[12] operated in the range 79–84 MHz, was used to measure the proton polarization. A Q-meter circuit contains a resonant LC circuit consisting of the NMR coil surrounding the crystal and a tunable capacitor outside the cryostat. In our apparatus, the capacitor was separated from the coil by one wavelength of coaxial cable. The LC voltage-response curve was displayed on an oscilloscope by synchronizing the oscilloscope sweep with an FM oscillator. The NMR frequency was determined by the magnetic field. The frequency of maximum voltage response was varied by tuning the capacitor until the proton resonance was centered at the top of the response curve.

The magnetic field was modulated with 1 G rms at 33 Hz, and a voltage proportional to the derivative of the NMR signal was obtained from a lock-in amplifier.[13] The derivative NMR signal was recorded in 30 sec by sweeping through the resonance at the rate of 6 kHz/sec. A second pen on the chart recorder monitored the amplitude of the rf voltage at the output of the Q-meter circuit.[14]

V. PROTON RESONANCE LINE SHAPES

The proton-resonance line shapes were taken with the (111) planes oriented perpendicular to the magnetic field. Figure 2 shows the derivative of the proton resonance for AlK alum No. 1, at thermal equilibrium and at 24% polarization. Each trace consists of an increasing frequency sweep on the left, followed by a decreasing frequency sweep. Figure 3 shows derivative recordings of polarized proton resonances for crystals No. 2 and No. 3, and both derivative and integral recordings for crystal No. 4. The peak-to-peak linewidth of the derivative signals differ for each crystal, and are listed in Table I.

The recordings show various amounts of fine structure. We observed that the line shape in alums did not change as the polarization increased. This makes it possible to calculate the proton polarization from the derivative signal, rather than having to measure the area under an integral curve.

Schmugge and Jeffries[6] have shown that when the proton polarization is high in LMN, the proton line shape is very asymmetrical, and entirely different from the thermal-equilibrium line shape. We observed a similar line-shape change in our LMN crystal.

VI. PROTON SPIN-LATTICE RELAXATION TIMES

The proton spin-lattice relaxation time $T_{1\rho}$ was measured by following the exponential decrease of the polarization with time, after turning off the microwave power. The rf oscillator at the NMR frequency was also turned off, except for 15-sec intervals every 3 min. The values of $T_{1\rho}$ at 19.5 kG and 0.93 K are given in Table I. $T_{1\rho}$ is plotted versus temperature in Fig. 4.

The solid curve in Fig. 4 represents the Gunter-Jeffries[6] measurements at 20 kG on an LMN crystal containing 1% Nd. The value of $T_{1\rho}$ for the LMN crystal we used was roughly $4\frac{1}{2}$ times shorter at 0.93 K than Gunter and Jeffries measured. This may be due to the unenriched Nd in our LMN crystal. The nuclear spins of the odd-odd Nd isotopes (20.5%) are relaxed very rapidly by hyperfine coupling, and may shorten the proton $T_{1\rho}$ by cross relaxation. The other possibility

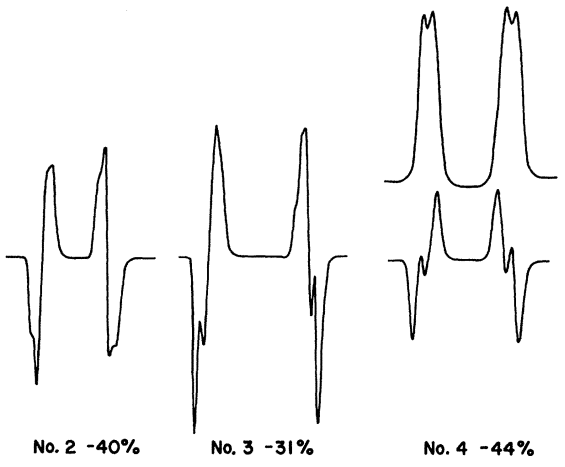

FIG. 3. Derivative proton NMR recordings for alum crystals Nos. 2–4 at the polarizations indicated. The integral NMR recording is shown above the derivative recording for crystal No. 4.

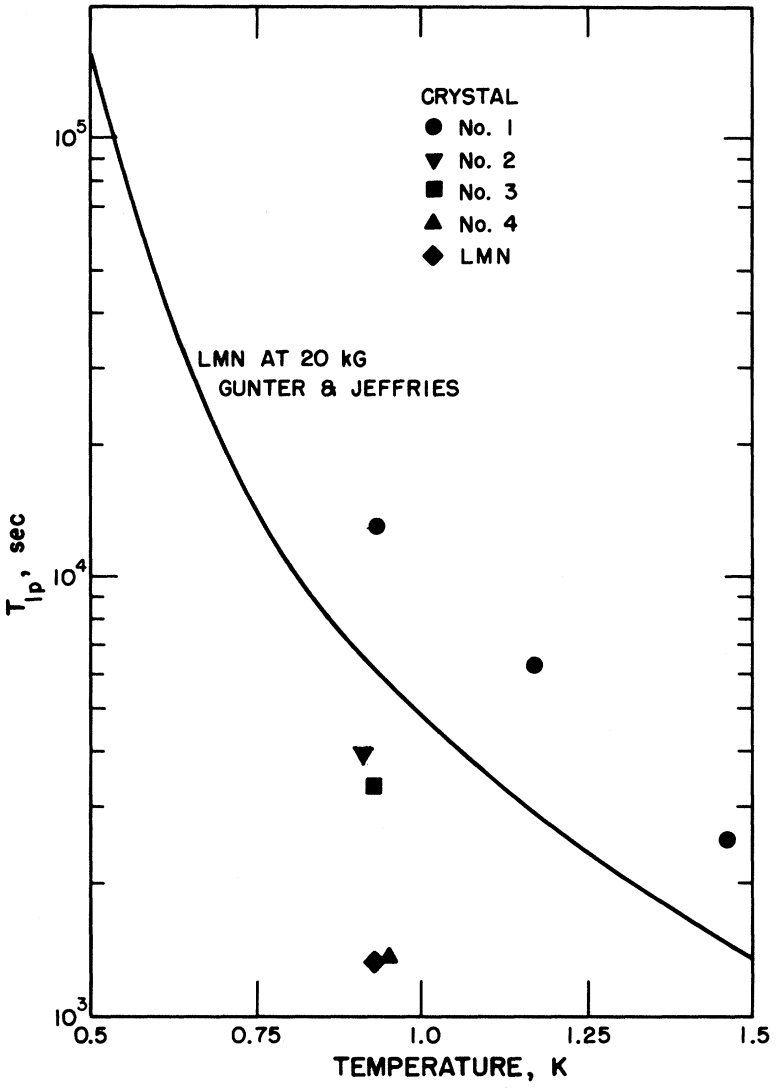

FIG. 4. Proton spin-lattice relaxation time T_{1p} at 19.5 kG and various temperatures. The solid curve for LMN is taken from Gunter and Jeffries (Ref. 6). The point labeled LMN is a measurement on our crystal, which contains unenriched Nd.

is the presence of unknown paramagnetic impurity in our LMN crystal.

Gunter and Jeffries extended their measurements on LMN down to 0.5 K, at which temperature T_{1p} equaled 40 h (at 19.5 kG). The relaxation time of alum crystal No. 1 was about twice as long as the solid curve in Fig. 4, at 0.93, 1.17, and 1.46 K (T_{1p} was 6350 and 2500 sec at the higher temperatures). We believe this long relaxation time was due to lower paramagnetic impurity content than in the other alum crystals. We also note that crystal No. 1 contained only $\frac{1}{3}$ the concentration of paramagnetic ions as LMN crystals containing 1% Nd. If the temperature dependence of T_{1p} in alums is the same as LMN between 0.5 and 1 K, then T_{1p} in crystal No. 1 will be about 3 days at 0.5 K. Such a long relaxation time would make pure AlK alum very useful for "storing" proton polarization.

Alum crystal No. 4 had an unusually short relaxation time. Spectrographic analysis of crystal No. 4 indicated that it contained 100-ppm copper impurity, which was not present in the other alum crystals. The Cu^{2+} ion is paramagnetic, but we were unable to detect Cu^{2+} using EPR (see PB).

VII. CALCULATION OF PROTON POLARIZATION

Proton polarization was calculated using the relation $P=EP_{\mathrm{TE}}$, where E is the enhancement and P_{TE} is the thermal-equilibrium (TE) polarization due to the Boltzmann distribution between the two proton Zeeman levels

$$P_{\mathrm{TE}}=\tanh(h\nu/2kT)\approx 2.40(\nu/T)\times 10^{-11}, \quad (13)$$

where h is Planck's constant, ν is the proton resonant frequency, k is Boltzmann's constant, and T is the temperature. In order to establish thermal equilibrium in a reasonable time, P_{TE} was measured at 1.5 K, where the proton relaxation time is shorter than at 1 K. At 19.4 kG and 1.5 K, P_{TE} equals 1.32×10^{-3}.

TABLE II. Conditions during dynamic proton polarization, and calculations based on the growth-rate curves. The g value for Cr^{3+} in alums is 1.977, and P_0 equaled 0.86; the g value of Nd^{3+} in LMN is 2.70, and P_0 equaled 0.94. Values in parentheses were obtained with the (110) planes perpendicular to the magnetic field.

Crystal	AlK No. 1	AlK No. 2	$AlNH_4$ No. 3	$AlNH_4$ No. 4	LMN
Temperature (K)	1.00	1.00	1.02	1.02	1.00
Magnetic field (kG)	18.932	19.575	19.553	19.593	19.598
Microwave frequency (GHz)	52.40	54.18	54.12	54.23	74.08
Microwave power (mW)	190	190	290	260	200
Field H_{1e} (mG)	84	84	102	97	73
Saturation S	31	32	50	92	480
Leakage factor f	0.0020	0.0026	0.0095	0.034	0.021
p_{max} (−%)	54	43	53	51(44)	77
p_s (−%)	64	50	58	55(60)	80
τ (min)	90	53	23	19(22)	10
B'	1.16	1.39	1.09	1.48	1.30
$S_{1/2}$	11	23	23	47	79
$S/(S+S_{1/2})$	0.74	0.58	0.68	0.66	0.86
$\sigma\times10^{-8}$	3.60	4.39	7.57	8.50	20.91
r_2 (Å)	35.9	28.4	34.7	40.1	25.1
r_1 (Å)	5.5	6.4	4.4	3.6	5.3

The proton polarization is proportional to the imaginary part χ_n'' of the dynamic nuclear susceptibility. If the resonance line shape and width do not change between the TE and enhanced polarizations, then the polarization is also proportional to the difference between the extreme values of $d\chi_n''/dH$. With magnetic field modulation, the output voltage V_s from the lock-in amplifier is written[15]

$$V_s = A V_{rf}^2 (d\chi_n''/dH), \tag{14}$$

where A is a constant and V_{rf} is the amplitude of the output voltage from the Q-meter circuit. With the understanding that V_{rf} is evaluated coincidentally with V_s, we write

$$P = A'[V_{s+}/V_{rf}^2 - V_{s-}/V_{rf}^2] = A'\Delta V_s/V_{rf}^2, \tag{15}$$

where A' is a constant, and V_{s+} and V_{s-} are the maximum and minimum values of V_s recorded while the rf oscillator is swept through resonance. The extreme values of V_s occur at approximately the same values of V_{rf}.[16] The equation we used to calculate the polarization is

$$P = P_{TE}\frac{[\Delta V_s/V_{rf}^2]_p}{[\Delta V_s/V_{rf}^2]_{TE}}, \tag{16}$$

where the subscript p refers to voltages measured when the protons were dynamically polarized.

VIII. POLARIZATION DEPENDENCE ON MAGNETIC FIELD

With the microwave frequency fixed at the frequency of a cavity mode, the steady-state proton polarization p_s becomes a function of the deviation ΔH from the magnetic field H_0 at which the allowed EPR transition occurs. We designate ΔH_0 that value of ΔH for which $|p_s|$ is a maximum. For narrow EPR lines, whose half-width δH is $\ll\Delta H_0$, dynamic-polarization theory gives

$$|\Delta H_0| = (\gamma_p/\gamma_e)H_0. \tag{17}$$

Leifson and Jeffries[17] find that when the EPR lines are so broad that the allowed and forbidden transitions are not well resolved, $|\Delta H_0|$ is larger than given by Eq. (17), by an amount dependent on the saturation factor S.

A plot of p versus ΔH for AlK alum No. 1 is given in Fig. 5. The half-width δH of the EPR line for this crystal is 10 G. The value of $|\Delta H_0|$ from Eq. (17)

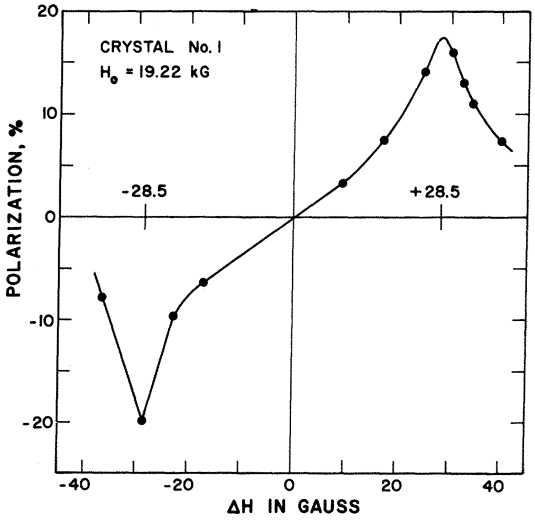

FIG. 5. Polarization after 45 min, as a function of the magnetic field displacement ΔH from the allowed EPR transition, for AlK alum No. 1. H_0 refers to the allowed EPR transition.

equals 1.538×19.22, or 29.6 G. The experimentally measured value of $|\Delta H_0|$ is 28.5±1 G. This result confirms that the theory of the solid effect for well-resolved EPR lines applies to the alum crystals.

The polarization growth rate in alum crystal No. 1 is very slow, and the values of p plotted in Fig. 5 are not p_s. Each point is the polarization which grew in during 45 min, at that magnetic field setting. The negative-polarization peak in Fig. 5 appears somewhat narrower than the positive-polarization peak.

IX. GROWTH-RATE CURVES AND CALCULATIONS

The experimental data used to evaluate the alum crystals come principally from the growth-rate curves for negative polarization shown in Figs. 6 and 7. By fitting the growth rates to Eq. (10), we were able to determine both p_s and τ. The solid lines in Figs. 6 and 7 correspond to the equations given. The maximum (negative) polarizations we measured are listed as $p_{\max}$ in Table II.

The performance of the LMN crystal, shown in Fig. 6, is superior to that of the $AlNH_4$ alums. This is because, at 19.6 kG, P_0 is 0.08 higher in LMN, and because the available microwave power was limited. The microwave factor $S/(S+S_{1/2})$ was 0.19 larger in LMN than the average for the $AlNH_4$ alums, which is a significant amount. The alum crystals require about three times as much microwave power as LMN for the same microwave factor. Both p_s and $1/\tau$ would have been larger in the alums if more microwave power had been available.

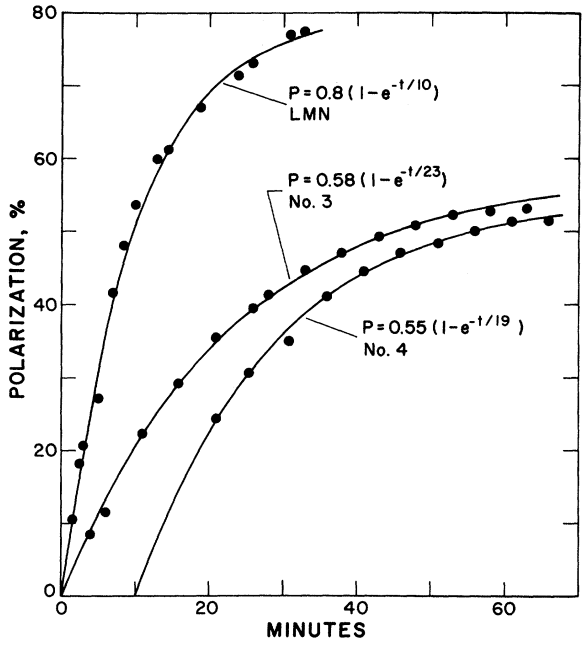

FIG. 6. Growth-rate curves for LMN and $AlNH_4$ alums Nos. 3 and 4. All polarizations are negative, and the growth-rate constant is given in minutes. The solid lines fit the equations given. The LMN crystal was oriented with the c axis perpendicular to magnetic field **H**, and the alum crystals with (111) planes perpendicular to **H**.

The LMN growth-rate curve was taken with the c axis of the crystal perpendicular to the magnetic field **H**. The growth-rate curves for the AlK and $AlNH_4$ alums were taken with the (111) planes perpendicular to **H**. The very long τ (90 min) for AlK alum No. 1 is related to the exceptionally long T_{1p}, by Eq. (11). We also polarized $AlNH_4$ alum No. 4 to −44% with the (110) planes perpendicular to **H**. In this orientation, the half-width δH of the EPR line is shown in PB to be only 3.5 G. The growth-rate curve in the (110) orientation fitted Eq. (10) with p_s equal to −60% and τ equal to 22 min.

A summary of our calculations is given in Table II. Successive lines in Table II follow the steps outlined in Sec. II. The large value of S for the LMN crystal follows in part from the narrow EPR linewidth, and in part from the long (phonon-bottlenecked) spin-lattice relaxation time T_{1e}.

There are two experimental difficulties in obtaining growth-rate curves. The first is to determine the exact magnetic field setting which gives the largest p_s and shortest τ. The second difficulty is to maintain precise tuning of all the equipment for the length of time required to obtain a growth curve. In view of these difficulties, and considering the wide variation among the crystals of the relaxation times T_{1e}, T_{2e}, and T_{1p}, we consider the values of B' and r_1 to be reasonably consistent. We expected r_1 would be larger than the closest ion-proton separation distance (∼2 Å), and approximately equal to r_1' (∼7 Å) in Jeffries's shell-of-influence model.[6] We expected B' would be closer to 1 than the values in Table II.

X. ALUM CRYSTALS AS POLARIZED PROTON TARGETS

LMN was widely used as a polarized proton target for several years, even though it contains only 3.17% hydrogen by weight. Interest has recently turned to hydrocarbon targets,[8] which contain ∼12% hydrogen by weight. For high-energy scattering experiments, the proton polarization is diluted by the ratio of bound protons to hydrogen nuclei. For these experiments, hydrocarbon targets, with a bound-to-free proton ratio ∼3.2 (butanol), have a very significant advantage over LMN and alums.

The alum crystals are similar to LMN, and their usefulness is probably limited to low-energy scattering experiments. LMN requires less microwave power, and has a larger P_0 in a given magnetic field, due to the larger g value (2.70) of the Nd^{3+} ion. At a high magnetic field (26 kG), and using a high-power microwave oscillator,[18] these advantages will provide only 5% additional polarization in LMN. The alums have the advantage of higher hydrogen density, by a factor of 1.61 for AlK alum and 1.97 for $AlNH_4$ alum. This means

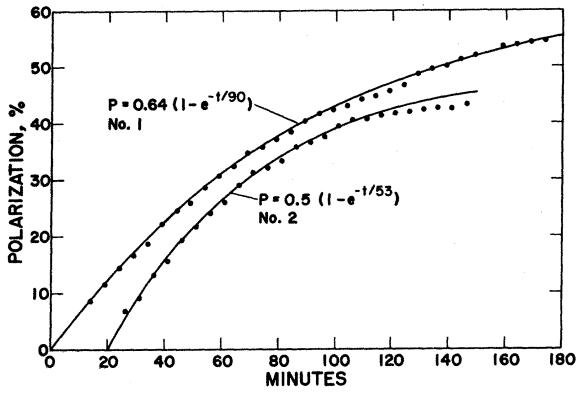

FIG. 7. Growth-rate curves for AlK alums Nos. 1 and 2. All polarizations are negative, and the growth-rate constants are given in minutes. The crystals were oriented with (111) planes perpendicular to **H**. The long growth-rate constant of No. 1 is related to the long relaxation time $T_{1\rho}$.

that an $AlNH_4$ alum target will expose to a beam approximately twice the number of polarized protons as LMN, for the same charged-particle energy loss in the target.

We expect 70–80% proton polarization can be achieved in alums at 26 kG with adequate microwave power. While hydrocarbon targets have twice the hydrogen density of $AlNH_4$ alum, they frequently have only 35–40% polarization. Unlike the hydrocarbons, the alum crystals are solid at room temperature, can be stored indefinitely at room temperature, and can be temperature cycled. It is convenient to measure the polarization which can be attained in an alum crystal before it is put in the beam, thus assuring that accelerator time is not wasted. A number of laboratories plan to cool their hydrocarbon targets with ^3He to temperatures below 1 K in order to obtain longer proton relaxation time $T_{1\rho}$ and higher polarization; this added complexity is not needed when using alum or LMN targets. Anyone designing a polarized proton target for low-energy scattering should consider the high hydrogen density of alums compared with LMN, and the convenience of alums compared to hydrocarbon targets.

ACKNOWLEDGMENTS

We thank Dr. J. E. Simmons, Dr. J. A. Jackson, and J. C. Martin for assistance with equipment used for the measurements.

* Work performed under the auspices of the U.S. Atomic Energy Commission.

[1] R. W. G. Wyckoff, *Crystal Structures*, 2nd ed. (Interscience, New York, 1951), Vol. 3.

[2] C. D. Jeffries, *Dynamic Nuclear Orientation* (Interscience, New York, 1963); A. Abragam and M. Borghini, in *Progress in Low Temperature Physics*, edited by C. J. Gorter (North-Holland, Amsterdam, 1964), Vol. IV, Chap. VIII.

[3] The EPR spectra of the crystals, and the ion spin-lattice relaxation times, are described in the preceding paper, Phys. Rev. B **2,** 4366 (1970), which we refer to as PB.

[4] B. Bleaney, Proc. Roy. Soc. (London) **A204,** 203 (1950).

[5] The LMN crystal was grown by the late Dr. T. R. Roberts. A nominal 1% of the lanthanum was replaced with "unenriched" Nd.

[6] C. D. Jeffries, University of California, Berkeley Technical Report No. UCB-34P20-T-1 (unpublished); T. J. Schmugge and C. D. Jeffries, Phys. Rev. **138,** A1785 (1965); T. E. Gunter and C. D. Jeffries, *ibid.* **159,** 290 (1967).

[7] M. Borghini, Phys. Rev. Letters **16,** 318 (1966).

[8] S. Mango, Ö. Runolfsson, and M. Borghini, Nucl. Instr. Methods **72,** 45 (1969); H. Glättli, M. Odehnal, J. Ezratty, A. Malinovski, and A. Abragam, Phys. Letters **29A,** 250 (1969); A. Masaike, H. Glättli, J. Ezratty, and A. Malinovski, *ibid.* **30A,** 63 (1969).

[9] M. Borghini, Phys. Letters **26A,** 242 (1968); Phys. Rev. Letters **20,** 419 (1968).

[10] M. Borghini, in *Proceedings of the Seventh International Conference on Low-Temperature Physics, 1960* (University of Toronto Press, Toronto, 1961).

[11] The aluminum concentrations were determined gravimetrically, and the chromium concentrations were determined by atomic absorption in a flame, using the 3578.7-Å chromium line. The concentrations were measured by Ross Gardner, Group CMB-1, Los Alamos Scientific Laboratory.

[12] A. Abragam, *The Principles of Nuclear Magnetism* (Oxford U. P., London, 1961), p. 75.

[13] Princeton Applied Research model HR-8.

[14] The NMR electronics are described in more detail in P. J. Bendt, J. A. Jackson, J. C. Martin, T. R. Roberts, and J. E. Simmons, Nucl. Instr. Methods **83,** 201 (1970).

[15] C. H. Schultz, Ph.D. thesis, University of California, Berkeley, 1964 (unpublished), issued as UCRL-11149 by the Office of Technical Services (U.S. Department of Commerce, Washington, D.C., 1964).

[16] Since V_{rf} is changing rapidly when Vs is maximum or minimum, the value we used for V_{rf}^2 is the product of V_{rf} at the center of the resonance and V_{rf} off to one side of resonance, as suggested in Ref. 15.

[17] O. S. Leifson and C. D. Jeffries, Phys. Rev. **122,** 1781 (1961).

[18] Available from Varian of Canada and Thomson-CSF Electron Tubes.